Geomechanics and Engineering, *Vol. 16, No. 3 (2018) 331-339*
DOI: https://doi.org/10.12989/gae.2018.16.3.331

Geomechanical study of well stability in high-pressure, high-temperature conditions

Seyyed Shahab Tabatabaee Moradi*, Nikolay I. Nikolaev[a], Inna V. Chudinova and Aleksander S. Martel

Well Drilling Department, Saint-Petersburg Mining University, 199106, Saint Petersburg, Russian Federation

(Received March 6, 2017, Revised December 30, 2017, Accepted May 12, 2018)

Abstract. Worldwide growth in hydrocarbon and energy demand is driving the oil and gas companies to drill more wells in complex situations such as areas with high-pressure, high-temperature conditions. As a result, in recent years the number of wells in these conditions have been increased significantly. Wellbore instability is one of the main issues during the drilling operation especially for directional and horizontal wells. Many researchers have studied the wellbore stability in complex situations and developed mathematical models to mitigate the instability problems before drilling operation. In this work, a fully coupled thermoporoelastic model is developed to study the well stability in high-pressure, high-temperature conditions. The results show that the performance of the model is highly dependent on the truly evaluated rock mechanical properties. It is noted that the rock mechanical properties should be evaluated at elevated pressures and temperatures. However, in many works, this is skipped and the mechanical properties, which are evaluated at room conditions, are entered into the model. Therefore, an accurate stability analysis of high-pressure, high-temperature wells is achieved by measuring the rock mechanical properties at elevated pressures and temperatures, as the difference between the model outputs is significant.

Keywords: well drilling; borehole instability; wellbore collapse failure; geomechanical model; HPHT

1. Introduction

One of the vital aspects of a successful well construction is wellbore stability, as in recent years many instability problems are reported. Wellbore instability issues are complicated and costly to solve and may endanger the whole drilling operation. Therefore, a comprehensive wellbore stability assessment is essential to mitigate the possible failure of the wellbore (Simangunsong *et al.* 2006, Tabatabaee Moradi *et al.* 2016, Zhu *et al.* 2016).

Wellbore stability studies require full understanding of the rock behavior around the wellbore. The rock behavior is determined by numerous factors, such as state of in-situ stresses, pore pressure, rock strength properties, temperature, pressure, drilling fluid characteristics and well trajectory specifications (azimuth and inclination). Among these factors, drilling fluid characteristics and well trajectory specifications are adjustable, while the other factors cannot be controlled (Aslannezhad *et al.* 2015).

Mechanical, thermal or chemical effects may alter the state of in-situ stresses. Mechanical effects are associated to the stress alternation around the wellbore caused by the rock removal during the drilling process. The drilling fluid should replace the drilled-out rock and surrounding rocks must burden the weight that was previously burdened by the removed rock (Khaksar Manshad *et al.* 2014). Chemical effects are related to the water adsorption in shale layers, where the shale swelling may jeopardize the borehole stability. Thermal effects are due to the temperature difference between the drilling fluid and the formation rock, which may induce a stress alternation at the wall of the wellbore (Farahani *et al.* 2006).

These effects have been analyzed in many papers and several mathematical models are developed to study the wellbore stability. The main models are pure elastic, poroelastic, thermoporoelastic and chemical. In recent years, thermoporoelastic models are widely used in borehole stability applications. These models describe the behavior of the rock under in-situ stress field coupled with the hydraulic and thermal effects.

Different circumstances are applied in the wellbore stability analyses. In the work of Zare *et al.* (2010), the mechanical stability analysis of directional wells is presented. Zhang *et al.* (2006) developed a wellbore stability model, which considers the mechanical, thermal and chemical effects. Using this model, the authors successfully optimized the well trajectory and drilling fluid formulation. Farahani *et al.* (2006) worked on a thermoporoelastic model and indicated the effects of pressure and temperature changes on the wellbore stability. Using a poroelastic model, Ma and Chen (2015) proposed a semi-analytical method to assess the failure areas around the wellbore for shale gas formations.

Some researchers worked on the wellbore instability problems in the HPHT (high-pressure, high-temperature) conditions. Worldwide growth in energy demand is driving the oil and gas companies to extract from deeper reservoirs with challenges of drilling in HPHT environments. Increasing number of projects in HPHT environments

*Corresponding author, Ph.D. Student
E-mail: s.sh.tabatabaee@gmail.com
[a]Ph.D.
E-mail: nikinik@mail.ru

http://www.techno-press.org/?journal=gae&subpage=7 ISSN: 2005-307X (Print), 2092-6219 (Online)

requires adjusting operations of the well construction process to the available hostile conditions (Tabatabaee Moradi *et al.* 2015).

Wu *et al.* (2011) analyzed the wellbore stability of a HPHT well located in south China. They investigated the effects of elevated pore pressure gradient (up to 1.95 g/cm^3) and temperature (up to 155˚C) and highlighted the significant role of coupled pore pressure and temperature effects on the wellbore stability. In the work of Liu *et al.* (2015), authors investigated the wellbore instability problems in HTHP fractured tight formations. Based on their research, critical mud weight window for oil-based muds, providing the stability of the HPHT wells, is calculated.

All the developed numerical and analytical models in the above researches can be used to evaluate the stability of the wellbore based on the available circumstances. However, it should be noted that the model performance is significantly affected by the input parameters to the model. Rock mechanical properties are considered as one of the main input parameters for all models. The mechanical parameters for most of the calculations are derived based on the experimental analyses on the rock sample in the normal conditions (in terms of temperature and pressure). Therefore, a better knowledge of rock mechanical behavior is crucial for stability analysis in HPHT conditions.

In this work, two sets of hypothetical rock mechanical properties (compressive strength (σ_c), elastic modulus (E), Poisson's ratio (ν), internal friction angle (∅) and cohesion (C)) in normal and HPHT conditions are entered into a thermoporoelastic model separately to analyze the wellbore stability in HPHT condition. The objective is to highlight the significance of rock mechanical properties evaluation in HPHT conditions for stability analysis of HPHT wells.

2. Model development

A thermoporoelastic model is used to analyze the stability of the wellbore in HPHT condition. A brief review of the model development is presented here. More details about the model development and equations are available in the works of Farahani *et al.* (2006) and Zhang *et al.* (2006).

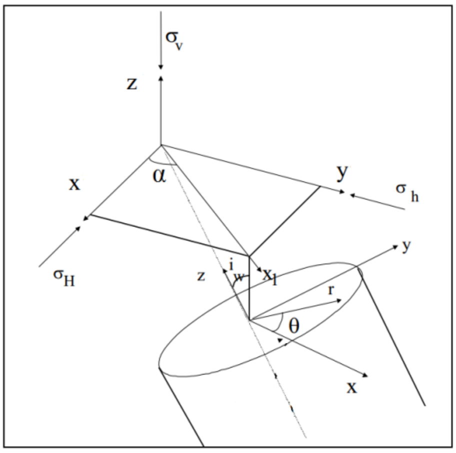

Fig. 1 Stress transformation for inclined borehole

Fig. 1 shows a simple model for an inclined borehole with a plain strain condition, in which the strain components ϵ_z, γ_{xz} and γ_{yz} are assumed to have zero values (Kanfar *et al.* 2015). The in-situ stresses and hydraulic effects induce stress around the borehole. By considering the law of Biot's effective stress, the components of the induced stress can be expressed in the cylindrical coordinate as follows (Bradely 1979, Lee *et al.* 2012)

$$\sigma_{rr} = \left(\frac{\sigma_x + \sigma_y}{2}\right)\left(1 - \frac{r_w^2}{r^2}\right) + \left(\frac{\sigma_x - \sigma_y}{2}\right)\left(1 + 3\,\frac{r_w^4}{r^4} - 4\,\frac{r_w^2}{r^2}\right)\cos 2\theta + \sigma_{xy}\left(1 + 3\,\frac{r_w^4}{r^4} - 4\,\frac{r_w^2}{r^2}\right)\sin 2\theta + \frac{r_w^2}{r^2}\,P_w - \alpha\,P\,(r,t) \tag{1}$$

$$\sigma_{\theta\theta} = \left(\frac{\sigma_x + \sigma_y}{2}\right)\left(1 + \frac{r_w^2}{r^2}\right) - \left(\frac{\sigma_x - \sigma_y}{2}\right)\left(1 + 3\,\frac{r_w^4}{r^4}\right)\cos 2\theta - \sigma_{xy}\left(1 + 3\,\frac{r_w^4}{r^4}\right)\sin 2\theta - \frac{r_w^2}{r^2}\,P_w - \alpha\,P\,(r,t) \tag{2}$$

$$\sigma_{zz} = \sigma_z - \nu\left[2\left(\sigma_x - \sigma_y\right)\frac{r_w^2}{r^2}\cos 2\theta + 4\,\sigma_{xy}\,\frac{r_w^2}{r^2}\sin 2\theta\right] - \alpha\,P\,(r,t) \tag{3}$$

$$\sigma_{r\theta} = \left(\frac{\sigma_x - \sigma_y}{2}\right)\left(1 - 3\,\frac{r_w^4}{r^4} + 2\,\frac{r_w^2}{r^2}\right)\sin 2\theta + \sigma_{xy}\left(1 - 3\,\frac{r_w^4}{r^4} + 2\,\frac{r_w^2}{r^2}\right)\cos 2\theta \tag{4}$$

$$\sigma_{\theta z} = \left(-\sigma_{xz}\sin\theta + \sigma_{yz}\cos\theta\right)\left(1 + \frac{r_w^2}{r^2}\right) \tag{5}$$

$$\sigma_{rz} = \left(-\sigma_{xz}\cos\theta + \sigma_{yz}\sin\theta\right)\left(1 - \frac{r_w^2}{r^2}\right) \tag{6}$$

where σ_{rr}, $\sigma_{\theta\theta}$ *and* σ_{zz} are the radial, hoop and axial stress respectively $\sigma_{r\theta}$, $\sigma_{\theta z}$, and σ_{rz} are components of the shear stress, P_w is the hydrostatic wellbore pressure, r_w is the borehole radius, $p(r,t)$ is the pore pressure profile, θ is the point location angle, ν is drained Poisson's ratio and α is the Biot's effective stress coefficient. σ_x, σ_y, σ_z, σ_{xy}, σ_{xz}, and σ_{yz} are the local stress distribution around the borehole in Cartesian coordinate, which are expressed based on the in-situ stresses in the virgin formation (Appendix A).

In addition, stresses induced by the temperature and pressure changes can be expressed as follows (Zhang *et al.* 2006)

$$\sigma_{rr} = \frac{E\,\alpha_m}{3\,(1-\nu)}\,\frac{1}{r^2}\int_{r_w}^{r} T^f(r,t)\,r\,dr + \frac{\alpha\,(1-2\nu)}{(1-\nu)}\,\frac{1}{r^2}\int_{r_w}^{r} P^f(r,t)\,r\,dr \tag{7}$$

$$\sigma_{\theta\theta} = -\frac{E\,\alpha_m}{3\,(1-\nu)}\left[\frac{1}{r^2}\int_{r_w}^{r} T^f(r,t) r\,dr - T(r,t)\right] - \frac{\alpha\,(1-2\nu)}{(1-\nu)}\left[\frac{1}{r^2}\int_{r_w}^{r} P^f(r,t) r\,dr - P(r,t)\right] \tag{8}$$

$$\sigma_{zz} = \frac{E\,\alpha_m}{3\,(1-\nu)}\,T^f(r,t) + \frac{\alpha\,(1-2\nu)}{(1-\nu)}\,P^f(r,t) \tag{9}$$

where α_m is the volumetric thermal expansion constant of the rock matrix, E is the Elastic (Young's) modulus and $T\,(r,t)$ is the temperature profile. $T^f\,(r,t)$ *and* $P^f(r,t)$ are defined as

$$T^f(r,t) = T\,(r,t) - T_0 \tag{10}$$

$$P^f(r,t) = P\,(r,t) - P_0 \tag{11}$$

T_0 and P_0 are initial formation temperature and pressure respectively. Difference between the drilling fluid and formation temperature induces direct thermal stresses in the formation. Besides that, this temperature change may alter the pore pressure profile around the borehole, as the pore fluid has a much larger coefficient of thermal expansion in comparison to the rock matrix (Choi *et al.* 2004, Li *et al.* 1998). Because of temperature variations, thermal stresses with magnitude of 10-50 MPa can be induced in the borehole wall (Liu *et al.* 2015).

Adding Eqs. (1)-(6) and Eqs. (7)-(9) by superposition principle, the complete thermoporoelastic model can be expressed as follows

$$\begin{aligned}\sigma_{rr} = &\left(\frac{\sigma_x+\sigma_y}{2}\right)\left(1-\frac{r_w^2}{r^2}\right) + \left(\frac{\sigma_x-\sigma_y}{2}\right)\\ &\left(1+3\,\frac{r_w^4}{r^4}-4\,\frac{r_w^2}{r^2}\right)\cos 2\theta\\ &+\sigma_{xy}\left(1+3\,\frac{r_w^4}{r^4}-4\,\frac{r_w^2}{r^2}\right)\sin 2\theta + \frac{r_w^2}{r^2}\,\mathrm{P_w}\\ &+\frac{E\,\alpha_m}{3\,(1-\nu)}\,\frac{1}{r^2}\int_{r_w}^{r} T^f(r,t) r\,dr\\ &+\frac{\alpha\,(1-2\nu)}{(1-\nu)}\,\frac{1}{r^2}\int_{r_w}^{r} P^f(r,t) r\,dr - \alpha\,P\,(r,t)\end{aligned} \tag{12}$$

$$\begin{aligned}\sigma_{\theta\theta} = &\left(\frac{\sigma_x+\sigma_y}{2}\right)\left(1+\frac{r_w^2}{r^2}\right) - \left(\frac{\sigma_x-\sigma_y}{2}\right)\\ &\left(1+3\,\frac{r_w^4}{r^4}\right)\cos 2\theta - \sigma_{xy}\left(1+3\,\frac{r_w^4}{r^4}\right)\sin 2\theta - \frac{r_w^2}{r^2}\,\mathrm{P_w}\\ &-\frac{E\,\alpha_m}{3\,(1-\nu)}\left[\frac{1}{r^2}\int_{r_w}^{r} T^f(r,t) r\,dr - T^f(r,t)\right]\\ &-\frac{\alpha\,(1-2\nu)}{(1-\nu)}\left[\frac{1}{r^2}\int_{r_w}^{r} P^f(r,t) r\,dr - P^f(r,t)\right] - \alpha\,P\,(r,t)\end{aligned} \tag{13}$$

$$\begin{aligned}\sigma_{zz} = &\,\sigma_z - \nu\left[2\left(\sigma_x-\sigma_y\right)\frac{r_w^2}{r^2}\cos 2\theta\right.\\ &\left.+4\,\sigma_{xy}\,\frac{r_w^2}{r^2}\sin 2\theta\right] + \frac{E\,\alpha_m}{3\,(1-\nu)}\,T^f(r,t)\\ &+\frac{\alpha\,(1-2\nu)}{(1-\nu)}\,P^f(r,t) - \alpha\,P\,(r,t)\end{aligned} \tag{14}$$

$$\begin{aligned}\sigma_{r\theta} = &\left(\frac{\sigma_x-\sigma_y}{2}\right)\left(1-3\,\frac{r_w^4}{r^4}+2\,\frac{r_w^2}{r^2}\right)\sin 2\theta\\ &+\sigma_{xy}\left(1-3\,\frac{r_w^4}{r^4}+2\,\frac{r_w^2}{r^2}\right)\cos 2\theta - \alpha\,P\,(r,t)\end{aligned} \tag{15}$$

$$\sigma_{\theta z} = \left(-\sigma_{xz}\sin\theta + \sigma_{yz}\cos\theta\right)\left(1+\frac{r_w^2}{r^2}\right) - \alpha\,P\,(r,t) \tag{16}$$

$$\sigma_{rz} = \left(-\sigma_{xz}\cos\theta + \sigma_{yz}\sin\theta\right)\left(1-\frac{r_w^2}{r^2}\right) - \alpha\,P\,(r,t) \tag{17}$$

To solve these equations and find the stress distribution around the borehole, temperature profile $T\,(r,t)$ and pore pressure profile $P(r,t)$ should be calculated. Formation temperature variations for a radial system can be found from the following diffusivity equation (Wang and Dusseault 2003)

$$\frac{\partial T}{\partial t} = c_0\,\Big(\frac{\partial^2 T}{\partial r^2}+\frac{1}{r}\,\frac{\partial T}{\partial r}\Big) + c_0'\left[\frac{\partial T}{\partial r}\,\frac{\partial P}{\partial r} + T\,\Big(\frac{\partial^2 P}{\partial r^2}+\frac{1}{r}\,\frac{\partial P}{\partial r}\Big)\right] \tag{18}$$

$$\frac{\partial T}{\partial t} = \underbrace{c_0\,\Big(\frac{\partial^2 T}{\partial r^2}+\frac{1}{r}\,\frac{\partial T}{\partial r}\Big)}_{A} + \underbrace{c_0'\left(\frac{\partial T}{\partial r}\,\frac{\partial P}{\partial r}\right)}_{B} + \underbrace{c_0'\,T\left(\frac{\partial^2 P}{\partial r^2}+\frac{1}{r}\,\frac{\partial P}{\partial r}\right)}_{C} \tag{19}$$

The expressions *A*, *B* and *C* demonstrate the effects of heat conduction, heat convection and pore pressure diffusion on the temperature variation respectively. In the case of low-permeability formations, the c_0' becomes much smaller than c_0 and consequently convective heat transfer effect on the temperature variations can be ignored. In most of the previous works, the models were developed based on this approximation and considered conductive heat effect only. c_0 and c_0' are conductive and convective thermal diffusivity coefficients, which are found from the following equations (Chen and Ewy 2005)

$$c_0 = \frac{\lambda}{\rho C_h} \tag{20}$$

$$c_0' = \frac{\kappa}{\varphi} \tag{21}$$

$$\kappa = \frac{k}{\mu} \tag{22}$$

where λ is thermal conductivity, ρ is the mass density, C_h is the specific heat capacity of the rock, φ is formation porosity, k is formation permeability and μ is the pore fluid viscosity. Pore pressure profile can be calculated from a similar diffusivity equation too

$$\frac{\partial P}{\partial t} = \underbrace{c\,(\frac{\partial^2 P}{\partial r^2} + \frac{1}{r}\frac{\partial P}{\partial r})}_{D} + \underbrace{c'\,\frac{\partial T}{\partial t}}_{E} \tag{23}$$

Expressions D and E represent the effects of pore pressure diffusion and temperature change on the pore pressure distribution. c and c' are hydraulic diffusivity and coupling coefficients, which can be defined by the Eqs. (24)-(25). For high-permeability formations the coefficient c' becomes much smaller than c and consequently the pore pressure variation due to the temperature change can be neglected.

$$c = \frac{2\,\kappa\,G\,B^2\,(1-\nu_u)^2(1-\nu)}{9\,(1-\nu_u)(\nu_u-\nu)} \tag{24}$$

$$c' = \frac{c}{\kappa}\left[\frac{2\alpha_m(\nu_u-\nu)}{B\,(1+\nu_u)(1-\nu)} + \varphi\,(\alpha_f - \alpha_m)\right] \tag{25}$$

In the above equations G is shear modulus, B is Skempton coefficient, ν_u is undrained Poisson ratio and α_f is the volumetric thermal expansion constant of pore fluid (Kurashige 1989, McTigue 1990). Eqs. (19) and (23) are solved numerically using an explicit finite difference method (FDM) to define the pore pressure and temperature profiles in the formation with respect to time (t) and space (r). Following spatial and time discretization are applied and a special computer program is developed to solve the equations

$$\begin{aligned}\frac{T_j^{n+1}-T_j^n}{\Delta t} &= c_0\,(\frac{T_{j+1}^n - 2\,T_j^n + T_{j-1}^n}{\Delta r^2} \\ &+ \frac{1}{r_w + j\Delta r}\,\frac{T_j^n - T_{j-1}^n}{\Delta r}) + c_0'\left[\frac{T_j^n - T_{j-1}^n}{\Delta r}\right. \\ &\frac{P_j^n - P_{j-1}^n}{\Delta r} + T\left(\frac{P_{j+1}^n - 2\,P_j^n + P_{j-1}^n}{\Delta r^2}\right. \\ &\left.\left.+ \frac{1}{r_w + j\Delta r}\,\frac{P_j^n - P_{j-1}^n}{\Delta r}\right)\right]\end{aligned} \tag{26}$$

$$\begin{aligned}\frac{P_j^{n+1}-P_j^n}{\Delta t} &= c\left(\frac{P_{j+1}^n - 2\,P_j^n + P_{j-1}^n}{\Delta r^2}\right. \\ &\left.+ \frac{1}{r_w + j\Delta r}\,\frac{P_j^n - P_{j-1}^n}{\Delta r}\right) + c'\,\frac{T_j^{n+1}-T_j^n}{\Delta t}\end{aligned} \tag{27}$$

The Eqs. (26)-(27) are solved for a semi-infinite model. Pressure at the wellbore wall is considered to be constant and equal to hydrostatic pressure of the drilling fluid (P_w). T_w is considered as the temperature at the wellbore wall for the inner boundary. The initial and boundary conditions for the inner and outer boundaries are summarized as follows

$$P\,(r_w,t) = P_w, \qquad T\,(r_w,t) = T_w \tag{28}$$

$$P\,(r_\infty,t) = P_0, \qquad T\,(r_\infty,t) = T_0 \tag{29}$$

$$P\,(r,0) = P_0, \qquad T\,(r,0) = T_0 \tag{30}$$

Calculated pore pressure and temperatures profiles are used in Eqs. (12)-(17) to find the stress alternation around the borehole. Because of the stress alternation and strength reduction of the rocks around the borehole the formation failure may occur. Two mechanisms of rock failure are shear failure (also called breakout or compressive failure) and tensile failure, which may result in borehole breakout, stuck pipe, loss of drilling fluid, low-quality cementing, sidetracking, drilling operation delay and etc. (Abdideh and Fathabadi 2013, Chen *et al.* 1997, Zhang *et al.* 2010). Therefore, a suitable failure criterion is required to assess the rock stability and predict its failure before the drilling process. The most used failure criteria are Mohr-Coulomb, Drucker-Prager, Mogi-Coulomb and modified Lade. Mohr-Coulomb failure criterion is considered as one of the oldest and simplest criteria, which has been used frequently to evaluate the compressive failure of the borehole wall. Drucker-Prager criterion is defined as the combination of the Mohr-Coulomb and Van-Mises criteria. In the Mohr–Coulomb criterion, the effect of intermediate principal stress is neglected, and therefore overestimated values of required minimum mud pressure are calculated. On the opposite, in the Drucker-Prager the effect of intermediate principal stress is exaggerated, and therefore underestimated values of required minimum mud pressure are calculated (Elyasi and Goshtasbi 2015). The Mogi-Coulomb failure criterion (Al-Ajmi and Zimmerman 2006, Ma *et al*. 2015) (Eq. (31)) is used in this work to assess the failure of the rock around the borehole, as it correctly takes into account the effect of intermediate principal stress and therefore shows more realistic results in comparison with the other criteria.

$$FC = \left(a + b\,\sigma_{m,2}\right) - \tau_{oct} \tag{31}$$

$$\tau_{oct} = a + b\,\sigma_{m,2} \tag{32}$$

FC is the rock failure criterion. a and b are constants related to rock properties, $\sigma_{m,2}$ is the mean stress and τ_{oct} is the octahedral shear stress

$$\sigma_{m,2} = \frac{\sigma_1 + \sigma_3}{2} \tag{33}$$

$$\tau_{oct} = \frac{1}{3}\sqrt{(\sigma_1-\sigma_2)^2 + (\sigma_2-\sigma_3)^2 + (\sigma_1-\sigma_3)^2} \tag{34}$$

$$a = \frac{2\sqrt{2}}{3}\,C\cos\emptyset \tag{35}$$

$$b = \frac{2\sqrt{2}}{3}\sin\emptyset \tag{36}$$

The rock will fail if FC becomes less than zero. In above expressions C is rock cohesion, $\emptyset$ is internal friction angle, σ_1, σ_2, and σ_3 are maximum, intermediate and minimum principal stresses respectively (Appendix B).

3. Results and discussion

The Eqs. (26)-(27) are solved using an explicit finite

Table 1 Used parameters for pore pressure and temperature profiles calculations (Simangunsong *et al.* 2006, Farahani *et al.* 2006)

Parameter	Value	Parameter	Value
dt	1 s	P_w	55 Mpa
dr	0.005 m	μ	1 cp
r_w	0.125 m	c_0	7.15×10^{-7} m^2/s
T_0	155 ° C	c_0'	4.94×10^{-9} m^2/Mpa.s
P_0	45 Mpa	c	3.36×10^{-9} m^2/s
T_w	55 ° C	c'	0.31 MPa/°C

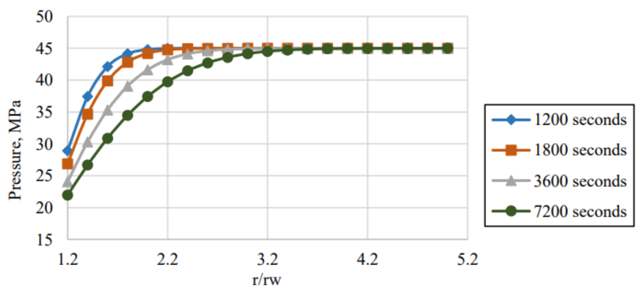

Fig. 2 Pressure profile at close distances to borehole

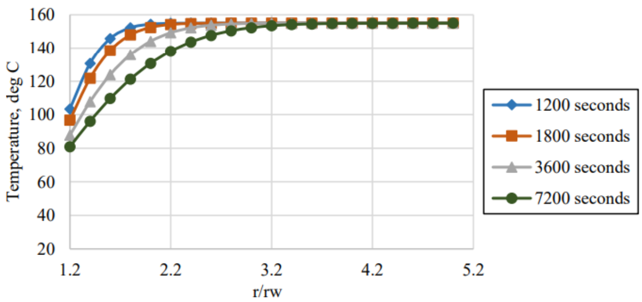

Fig. 3 Temperature profile at close distances to borehole

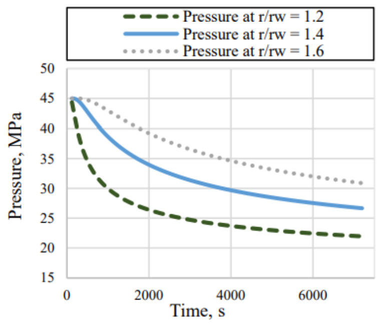

(a) Pore pressure profile

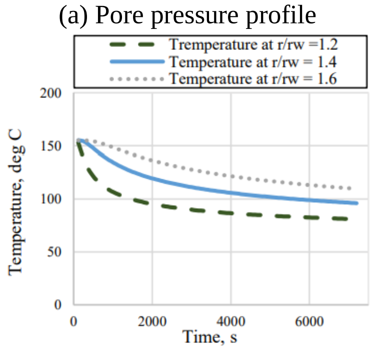

(b) Temperature profile

Fig. 4 Pressure and temperature profile with respect to time

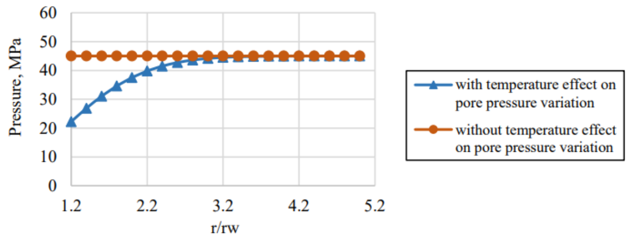

Fig. 5 Temperature effect on pore pressure variation

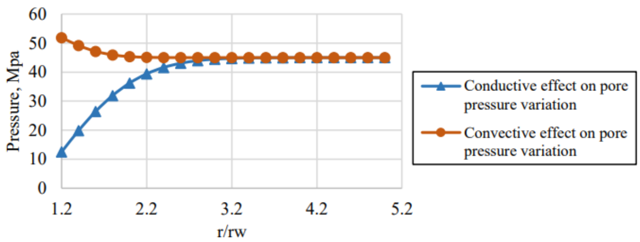

Fig. 6 Conductive and convective effects on pore pressure variation at 7200 s

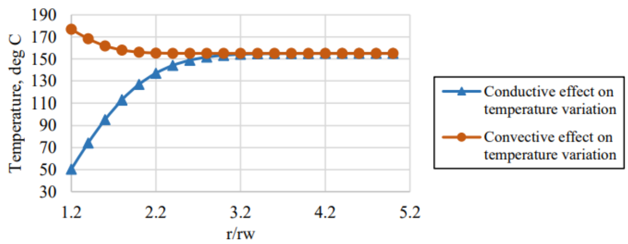

Fig. 7 Conductive and convective effects on temperature variation at 7200 s

difference method for the input parameters in Table 1.

The pore pressure and temperature profiles near the wellbore are calculated at four different times and shown in Figs. 2 and 3. Figs 4(a)-4(b) show the temperature and pore pressure variations with respect to time at close distances to the wellbore. By increasing the radial distance from the wellbore, the pore pressure and temperature reach their initial values.

As the formation is considered to be situated at HPHT condition, the effect of temperature on the pore pressure profile cannot be ignored, i.e., the c' cannot take the zero value. Fig. 5 shows the pore pressure profile with and without temperature effect.

To better understand the conductive and convective effects on the temperature and pore pressure variations, they are shown separately in Figs. 6 and 7. As the equations are solved for a low-permeability formation, the convective heat transfer have a minor influence on the temperature and pore pressure variations, and therefore it may be neglected.

The pore pressure and temperature profiles are calculated for different values of wellbore pressure (P_w). Theses profiles are used in Eqs. (12)-(17) to analyze the stress distribution around the borehole, and finally evaluate the minimum required density of the drilling fluid, which prevents from borehole collapse.

To highlight the significant role of truly evaluated mechanical properties in HPHT conditions in borehole stability analysis, two sets of mechanical properties are used

Table 2 Input mechanical properties for stability calculations (Aslannezhad *et al.* 2015, Khaksar Manshad *et al.* 2014, Wu *et al.* 2011)

Mechanical property	Case I (mechanical properties are evaluated at normal conditions)	Case II (effects of HPHT condition on the mechanical properties are considered)
Compressive strength (MPa)	90	200
E (MPa)	3336	3386
ν (-)	0.27	0.34
C (MPa)	40	22
∅ (deg)	32	32

Table 3 Other used parameters for stability calculations (Aslannezhad *et al.* 2015, Khaksar Manshad *et al.* 2014, Wu *et al.* 2011)

Parameter	Value	Parameter	Value
i	0-90 deg	T_0	155 ˚C
α_a	0-180 deg	P_0	45 MPa
S_v	75 MPa	α	0.9
S_H	67 MPa	α_m	3.5×10^{-5} 1/°C
S_h	60 MPa	Reservoir depth	5000 m

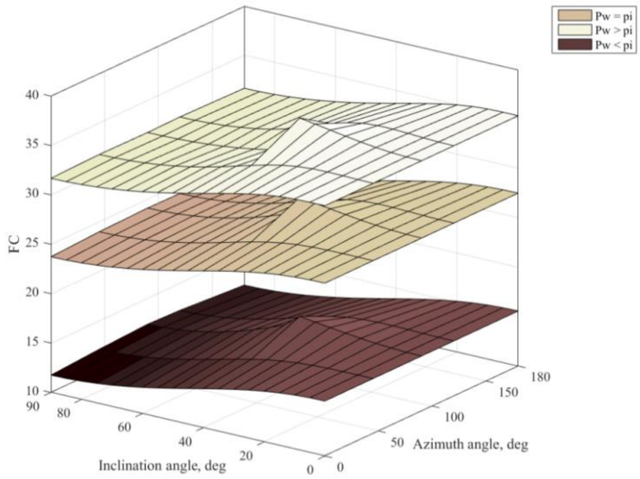

Fig. 8 Evaluated FC for case I

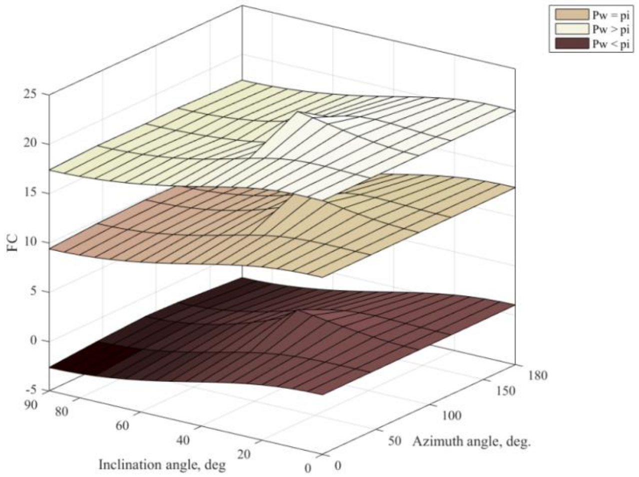

Fig. 9 Evaluated FC for case II

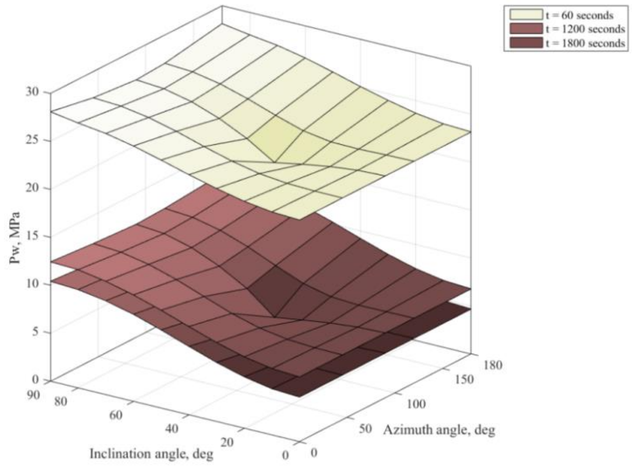

Fig. 10 Calculated minimum mud weight for case I

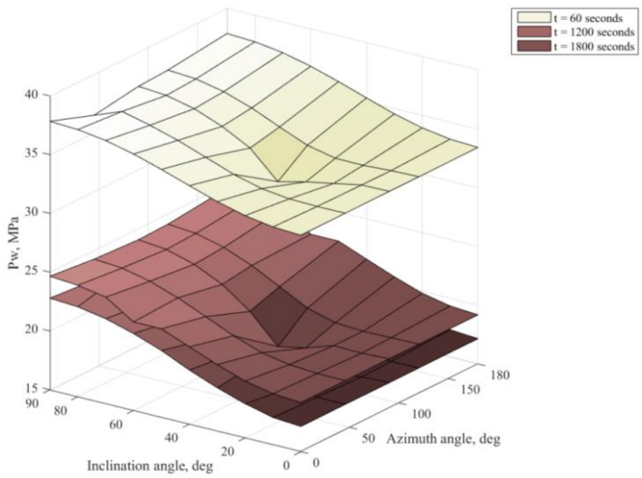

Fig. 11 Calculated minimum mud weight for case II

in the calculations and the results are compared together. The considered mechanical properties are compressive strength (σ_c), elastic modulus (E), Poisson's ratio (ν), internal friction angle (∅) and cohesion (C). At elevated temperatures and pressures, the value of these mechanical properties change. The combined effect of temperature and pressure on these properties is complex and variable; however, in some researches the general trend of the mechanical properties variation versus temperature and pressure is presented. Using these general trends, two hypothetical sets of mechanical properties are assumed and used in the calculations: case I, in which the mechanical properties are assumed to be evaluated at normal temperature and pressure condition and case II, in which the mechanical properties are affected by elevated temperature and pressure. The values of these properties in normal and HPHT conditions are presented in Table 2. The other required input parameters for stress distribution calculations are presented in Table 3.

The FC values are calculated for both cases. Three possible drilling situations are considered (overbalanced, underbalanced and balanced) and the wellbore stability for

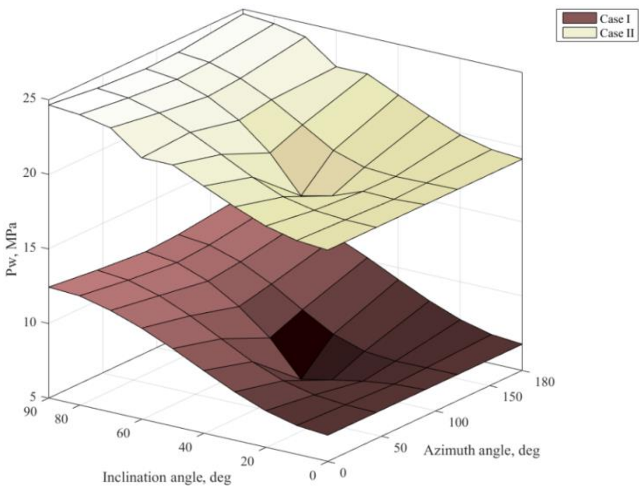

Fig. 12 Case I and case II comparison

different inclination and azimuth angles is evaluated. The result are presented in Figs. 8 and 9. As it was expected, overbalanced drilling secures the most stable well at different times from the drilling operation beginning.

The minimum required mud weight, which prevents from wellbore collapse is calculated for both cases and represented in Figs. 10 and 11 for three different times (t = 60, 1200 and 1800 seconds). As it is evident from the figures the most stable well trajectory for both cases at different times of 60, 1200 and 1800 seconds can be achieved with inclination and azimuth angles of 40 and 90 degrees respectively at the given depth. It should be noted that by passing time, the well becomes more stable.

To understand the significance of truly evaluated mechanical properties at HPHT conditions, the result of stability analyses for both cases are compared (Fig. 12). As it is evident from the figure, in case I the underestimated values of minimum required mud weights are calculated, which may endanger the whole drilling operation. Therefore, for stability analysis in HPHT condition, it is required to evaluate the input mechanical properties at elevated temperatures and pressures to mitigate this risk.

4. Conclusions

Based on the wellbore stability analysis at different inclination and azimuth angles and for normal and HPHT conditions, the following conclusions can be made:

• The temperature has a major effect on the pore pressure and temperature variations around the wellbore, and thus cannot be ignored in stability calculations.

• As in this work the stability analysis is conducted for a low permeability rock, the convective effect has a minor effect on the pore pressure and temperature variations around the borehole.

• The most stable well can be drilled with inclination and azimuth angles of 40 and 90 degrees respectively for both cases at the given depth.

• The mechanical properties are one of the main input parameters for the stability analysis using different stress distribution models.

• For HPHT applications, the wellbore stability is usually estimated using the mechanical properties, which are calculated by laboratory measurements in normal temperatures and pressures. This may lead to underestimating the required minimum mud weight, which prevents from wellbore collapse. A fully successful wellbore stability study can be achieve by measuring the rock mechanical properties in the same pressure and temperature condition as the drilled well.

Acknowledgements

The authors would like to thank the staff of the well drilling department, Saint-Petersburg Mining University for their support.

References

Abdideh, M. and Fathabadi, M.R. (2013), "Analysis of stress field and determination of safe mud window in borehole drilling (case study: SW Iran)", *J. Petrol. Explor. Prod. Technol.*, **3**(2), 105-110.

Al-Ajmi, A.M. and Zimmerman, R.W. (2006), "Stability analysis of vertical boreholes using the Mogi-Coulomb failure criterion", *Int. J. Rock Mech. Min. Sci.*, **43**(8), 1200-1211.

Aslannezhad, M. and Jalalifar, H. (2015), "Determination of a safe mud window and analysis of wellbore stability to minimize drilling challenges and non-productive time", *J. Petrol. Explor. Prod. Technol.*, **6**(3), 493-503.

Bradely, W.B. (1979), "Failure of inclined boreholes", *J. Energy Resour. Technol.*, **101**(4), 232-239.

Chen, G. and Ewy, R.T. (2005), "Thermoporoelastic effect on wellbore stability", *SPE J.*, **10**(2), 121-129.

Chen, X. Tan, C.P. and Haberfield, C.M. (1997), "Guidelines for efficient wellbore stability analysis", *Int. J. Rock Mech. Min. Sci.*, **34** (3-4), 50.e1-50.e14.

Choi, S.K., Tan, C.P. and Freij-Ayoub, R. (2004), *A Coupled Mechanical-Thermal-Physico-Chemical Model for the Study of Time-Dependent Wellbore Stability in Shales*, in *Elsevier Geo-Engineering Book Series*, Elsevier, 581-586.

Elyasi, A. and Goshtasbi, K. (2015), "Using different rock failure criteria in wellbore stability analysis", *Geomech. Energy Environ.*, **2**, 15-21.

Farahani, H.S., Yu, M., Miska, S.Z., Takach, N.E. and Chen, G. (2006), "Modeling transient thermo-poroelastic effects on 3D wellbore stability", *Proceedings of the SPE Annual Technical Conference and Exhibition*, Texas, U.S.A., September.

He, S., Wang, W., Tang, M., Hu, B. and Xue, W. (2014), "Effects of fluid seepage on wellbore stability of horizontal wells drilled underbalanced", *J. Nat. Gas Sci. Eng.*, **21**, 338-347.

Kanfar, M.F., Chen, Z. and Rahman, S.S. (2015), "Effect of material anisotropy on time-dependent wellbore stability", *Int. J. Rock Mech. Min. Sci.*, **78**, 36-45.

Kurashige, M. (1989), "A thermoelastic theory of fluid-filled porous materials", *Int. J. Solids Struct.*, **25**(9), 1039-1052.

Lee, H., Ong, S.H., Azeemuddin, M. and Goodman, H. (2012), "A wellbore stability model for formations with anisotropic rock strengths", *J. Petrol. Sci. Eng.*, **96**, 109-119.

Li, X., Cui, L. and Roegiers, J.C. (1998), "Thermoporoelastic analyses of inclined boreholes", *Proceedings of the SPE/ISRM Rock Mechanics in Petroleum Engineering*, Trondheim, Norway, July.

Liu, M., Jin, Y., Lu, Y., Chen, M. and Wen, X. (2015), "Oil-based critical mud weight window analyses in HTHP fractured tight formation", *J. Petrol. Sci. Eng.*, **135**, 750-764.

Ma, T. and Chen, P. (2015), "A wellbore stability analysis model with chemical-mechanical coupling for shale gas reservoirs", *J. Nat. Gas Sci. Eng.*, **26**, 72-98.

Ma, T., Chen, P., Yang, C. and Zhao, J. (2015), "Wellbore stability analysis and well path optimization based on the breakout width model and Mogi-Coulomb criterion", *J. Petrol. Sci. Eng.*, **135**, 678-701.

Manshad, A.K., Jalalifar, H. and Aslannejad, M. (2014), "Analysis of vertical, horizontal and deviated wellbores stability by analytical and numerical methods", *J. Petrol. Explor. Prod. Technol.*, **4**(4), 359-369.

McTigue, D.F. (1990), "Flow to a heated borehole in porous, thermoelastic rock: analysis", *Water Resour. Res.*, **26**(8), 1763-1774.

Moradi, S.S.T., Ghasemi, M.F., Nikolaev, N.I. and Lykov, Y.V. (2016), "Effect of fault stress regime on the mechanical stability of horizontal boreholes", *Proceedings of the 4th International Conference GeoBaikal 2016: From East Siberia to the Pacific—Geology, Exploration and Development*, Irkutsk, Russia, August.

Simangunsong, R.A., Villatoro, J.J. and Davis, A.K. (2006), "Wellbore stability assessment for highly inclined wells using limited rock-mechanics data", *Proceedings of the SPE Annual Technical Conference and Exhibition*, Texas, U.S.A., September.

Tabatabaee Moradi, S.S., Nikolaev, N.I. and Naseri, Y. (2015), "Developing high resistant cement systems for high-pressure, high-temperature applications", *Proceedings of the SPE Russian Petroleum Technology Conference*, Moscow, Russia, October.

Wang, Y. and Dusseault, M.B. (2003), "A coupled conductive-convective thermo-poroelastic solution and implications for wellbore stability", *J. Petrol. Sci. Eng.*, **38**(3-4), 187-198.

Wu, B., Wu, B., Zhang, X. and Jeffrey, R.G. (2011), "Wellbore stability analyses for HPHT wells using a fully coupled thermo-poroelastic model", *Proceedings of the SPE Asia Pacific Oil and Gas Conference and Exhibition*, Jakarta, Indonesia, September.

Zare, M.R., Shadizadeh, S.R. and Habibnia, B. (2010), "Mechanical stability analysis of directional wells: a case study in Ahwaz oilfield", *Proceedings of the 34th Annual SPE International Conference and Exhibition*, Tinapa, Calabar, Nigeria, July-August.

Zhang, J., Yu, M., Al-Bazali, T.M., Ong, S., Chenevert, M.E., Sharma, M.M. and Clark, D.E. (2006), "Maintaining the stability of deviated and horizontal wells: Effects of mechanical, chemical, and thermal phenomena on well designs", *Proceedings of the SPE International Oil & Gas Conference and Exhibition*, Beijing, China, December.

Zhang, L., Cao, P. and Radha, K.C. (2010), "Evaluation of rock strength criteria for wellbore stability analysis", *Int. J. Rock Mech. Min. Sci.*, **47**(8), 1304-1316.

Zhu, X., Liu, W. and Zheng, H. (2016), "A fully coupled thermo-poroelastoplasticity analysis of wellbore stability", *Geomech. Eng.*, **10**, 437-454.

CC

Appendix A

Local stress distribution around the borehole in Cartesian coordinate are expressed based on the in-situ stresses in the virgin formation as follows (He *et al.* 2014)

$$\sigma_{\mathrm{x}} = (\sigma_{\mathrm{H}}\, cos^2\alpha_a + \sigma_{\mathrm{h}}\, sin^2\alpha_a) cos^2 i + \sigma_{\mathrm{v}}\, sin^2 i \quad (37)$$

$$\sigma_{\mathrm{y}} = \sigma_{\mathrm{H}}\, sin^2\alpha_a + \sigma_{\mathrm{h}} cos^2\alpha_a \quad (38)$$

$$\sigma_{\mathrm{z}} = (\sigma_{\mathrm{H}}\, cos^2\alpha_a + \sigma_{\mathrm{h}}\, sin^2\alpha_a) sin^2 i + \sigma_{\mathrm{v}}\, cos^2 i \quad (39)$$

$$\sigma_{\mathrm{xy}} = 0.5\, (\sigma_{\mathrm{h}} - \sigma_{\mathrm{H}})\; sin\, 2\alpha_a \cos i \quad (40)$$

$$\sigma_{\mathrm{xz}} = 0.5\, (\sigma_{\mathrm{H}}\, cos^2\alpha_a - \sigma_{\mathrm{h}}\, sin^2\alpha_a - \sigma_{\mathrm{v}})\; sin\, 2i \quad (41)$$

$$\sigma_{\mathrm{yz}} = 0.5\, (\sigma_{\mathrm{h}} - \sigma_{\mathrm{H}})\; sin\, 2\alpha_a \sin i \quad (42)$$

Appendix B

Maximum, intermediate and minimum principal stresses can be calculated from the following known equations

$$\sigma_1 = \frac{1}{2}(\sigma_{\mathrm{zz}} + \sigma_{\theta\theta} + \sqrt{(\sigma_{zz} - \sigma_{\theta\theta})^2 + 4\,\sigma_{\theta z}^2}) \quad (43)$$

$$\sigma_3 = \frac{1}{2}(\sigma_{\mathrm{zz}} + \sigma_{\theta\theta} - \sqrt{(\sigma_{zz} - \sigma_{\theta\theta})^2 + 4\,\sigma_{\theta z}^2}) \quad (44)$$

$$\sigma_2 = \sigma_{\mathrm{rr}} \quad (45)$$